# Role of Elastic Stress in Statistical and Scaling Properties of Elastic Turbulence

Teodor Burghelea, Enrico Segre, and Victor Steinberg
*Department of Physics of Complex Systems, Weizmann Institute of Science, Rehovot, 76100 Israel*
(Received 25 October 2005; published 31 May 2006)

The role of elastic stress in statistical and scaling properties of elastic turbulence in a polymer solution flow between two disks is discussed. The analogy with a small-scale magnetodynamics and a passive scalar turbulent advection in the Batchelor regime is used to explain the experimentally observed statistical properties, the flow structure, and the scaling of elastic turbulence. The emergence of a new length scale, namely, the boundary layer thickness, is observed and studied.

DOI: 10.1103/PhysRevLett.96.214502 PACS numbers: 47.27.−i, 47.50.−d, 83.50.−v

The discovery of elastic turbulence, a random flow in a dilute polymer solution at arbitrary low Reynolds numbers, Re, opens up a new possibility to study, both experimentally and theoretically, the role of elastic stress in flow dynamics [1]. The elastic stress is the main source of nonlinearity in low Re polymer solution flows. An elastic instability and further elastic turbulence show up when the elastic energy overcomes the dissipation due to polymer relaxation [1,2].

Elastic turbulence leads to sharp growth in flow resistance, exhibits an algebraic decay in a wide range of scales in the velocity power spectra, and provides a way for effective mixing [1–3]. These properties are analogous to those shown by hydrodynamic turbulence. This formal similarity is the reason to coin this random flow as elastic turbulence. However, it does not imply a similarity in the physical mechanisms that underlie the two kinds of random motion. Indeed, contrary to inertial turbulence at high Re that occurs due to large Reynolds stress [4], large elastic stress is the main source of nonlinearity and elastic turbulence in low Re polymer solution flows [5]. One can suggest that in an elasticity driven random flow the elastic stress tensor, $\boldsymbol{\tau}_p$, should be the object of primary importance and interest. So, it may be appropriate to view the elastic turbulence as turbulence of the $\boldsymbol{\tau}_p$ field. In this case it would be more relevant and quite instructive to explore the spatial structure and temporal distribution of the elastic stress. But there is currently no technique to conduct local measurements of $\boldsymbol{\tau}_p$ in a turbulent flow. On the other hand, properties of the $\boldsymbol{\tau}_p$ field in the boundary layer can be inferred from measurements of an injected power, whereas its local properties can be evaluated from measurements of spatial and temporal distributions of velocity gradients.

The crucial step towards a theoretical description of elastic turbulence is to relate the dynamics of $\boldsymbol{\tau}_p$ to the dynamics of a vector field with a linear damping [6–8]. As was shown [6], the elastic stress tensor can be described as uniaxial, (i.e., $\tau_{ik} = B_i B_k$), if the contribution into $\boldsymbol{\tau}_p$ due to thermal fluctuations and polymer nonlinearity can be neglected. Then one can write an equation for $B_i$ in a form that is similar to the equation for magnetic field in magneto-hydrodynamics (MHD) [7]. Thus, in the case of a visco-elastic flow one gets

$$\partial_t \mathbf{B} + (\mathbf{V}\cdot\nabla)\mathbf{B} = (\mathbf{B}\cdot\nabla)\mathbf{V} - \mathbf{B}/\lambda, \tag{1}$$

where $\lambda$ is the polymer relaxation time. The distinction with MHD shows up only in the relaxation term that replaces the diffusion one. Otherwise, elastic turbulence is analogous to a small-scale fast viscosity-dominated magnetodynamics. The latter results from random stretching of the (nearly) frozen-in magnetic field lines by an advecting random flow. In numerical simulations the magnetodynamics shows features very similar to those observed in elastic turbulence [9]. Equation (1), when complemented by the equation of motion written for $\mathrm{Re} \ll 1$ as

$$\nabla P = \rho(\mathbf{B}\cdot\nabla)\mathbf{B} + \eta\nabla^2\mathbf{V}, \tag{2}$$

and by the boundary conditions, reveals elastic instability at $\mathrm{Wi} = \mathrm{Wi}_c > 1$ [10,11]. Here $\mathrm{Wi} = \dot{\gamma}\lambda$ is the Weissenberg number. At $\mathrm{Wi} > \mathrm{Wi}_c$ the instability eventually results in chaotic, statistically steady dynamics. According to Ref. [6], a statistically steady state occurs due to the backreaction of stretched polymers, [or the elastic stress in Eq. (2)] on the velocity field. The latter leads to a saturation of $\boldsymbol{\tau}_p$ even for linear relaxation [6]. On the other hand, the velocity gradients become smaller with decreasing scale. This means that large-scale fluctuations dominate in the flow. Their dynamics is determined by the nonlinear interaction of modes on scales of the order of the system size. So, the elastic stress is estimated as

$$\tau_p = B^2 \sim (\eta/\rho)\nabla V \sim \frac{\eta/\rho}{\lambda}. \tag{3}$$

The fluctuating velocity field and stress tensor (or $\boldsymbol{B}$) can both be decomposed into large-scale, $\boldsymbol{V}$ and $\boldsymbol{B}$, and small-scale, $\boldsymbol{v}$ and $\boldsymbol{B}'$, components. Then the leading mechanism for generation of the small scales is the advection of a fluid element, which carries the elastic stress by the fluctuations of the large-scale flow. Thus, this problem is reduced to a linearly damped vector field problem with a dynamo effect due to field stretching. The analysis of the equations for the

 

small-scale fluctuations of both fields derived from Eqs. (1) and (2) leads to a powerlike decaying velocity spectrum in the wave number domain, $k$. In a spherical representation this has a form $E(k) \sim k^{-\alpha}$ with $\alpha > 3$ [7], in a good agreement with the experimental values $\alpha = 3.3$–$3.6$ [1–3]. The mechanism of stretching and folding of the elastic stress field by a random advecting flow with the dynamo effect and homogeneous attenuation of the stress field is rather general. It is directly related to the Batchelor regime considered a long time ago [12], where a passive scalar is advected by a spatially smooth and random in time flow. Since in elastic turbulence the velocity spectrum decays faster than $k^{-3}$, the exponent of both the velocity and velocity gradients are determined by the vessel size. This explains why the elastic turbulent flow is spatially smooth, strongly correlated on the vessel size scale and random in time. This is the main feature of the Batchelor regime in hydrodynamic turbulence at scales below the dissipative one [12]. By investigating the shape of the cross-correlation function of the velocity field in elastic turbulence it was found that the linear velocity field (locally uniform rate of strain) well approximates it. This is a direct confirmation of the fact that elastic turbulence is a single-scale, spatially smooth, and random in time flow [13].

In this Letter we elucidate the role of the elastic stress in the statistics and scaling of torque, in the statistics and saturation of rms of vorticity (velocity gradients) in the bulk, and in the structure and scaling of the velocity and velocity gradient fields in the bulk and in the boundary layer in elastic turbulence.

The experiments were conducted in a cylindrical container mounted on a commercial rheometer (AR-1000 from TA Instruments) with the rotating upper disk attached to its shaft. The latter allowed precise control (within 0.5%) of the disc angular velocity, $\Omega$, measurements of the torque, $T$, and torque fluctuations ($\Omega$ mode), or control of $T$ and measurements of $\Omega$ ($T$ mode). The radii of the upper and the lower plates were $R_i = 4.8$ cm and $R_c = 4.9$ cm, respectively. They were separated by $d = 2$ cm unless otherwise stated. For a swirling flow between disks, the shear rate can be defined as $\dot{\gamma} = \frac{\Omega R_c}{d}$. As a working fluid, we used a water-saccharose solution of 80 ppm by weight of high molecular weight polyacrylamide (Mw = 18Mda, from Polysciences). As a solvent, 65% by weight of saccharose in water was used, unless otherwise stated. The viscosities of the solvent and of the polymer solution at 22 °C were $\eta_s = 113.8$ mPa s and $\eta = 137.7$ mPa s, respectively. The polymer relaxation time obtained from small oscillation measurements varies as $\lambda \propto \dot{\gamma}^{-0.3}$ in the range of shear rates $\dot{\gamma} = 0.4$–$3.6$ s$^{-1}$, being $\lambda = 3.8$ s at $\dot{\gamma} = 2$ s$^{-1}$ [14]. We conducted laser Doppler velocimetry (LDV) measurements of azimuthal and vertical velocity components (two-component Dantec LDA) and particle image velocimetry (PIV) in a horizontal plane. In the latter measurements the cell was illuminated laterally by a thin laser sheet through the transparent walls of the fluid container between the plates. The sheet was 30 $\mu$m in the center and about 130 $\mu$m thick at the edges of the setup. As flow tracers, 10 $\mu$m fluorescent beads were used. We acquired 2000 pairs of flow images with a digital camera (PixelFly from PCO with 12 bit and $640 \times 512$ pixels resolution) every 120 ms with a time delay between consecutive images of 40 ms.

The fluctuations of the injected power, $P = T\Omega$, were measured for different Wi in the elastic turbulence regime in two modes: $\Omega$ mode ($P_\Omega$) and $T$ mode ($P_T$). Probability distribution functions (PDFs) of $P_\Omega$, normalized by the maximum probability, are based on $1.8 \times 10^5$ data points for each value of Wi and presented for different Wi in Fig. 1. We made three observations. First, the PDFs collapse on a single curve in the reduced variables $\delta P_\Omega / P_\Omega^{\rm rms}$, where $\delta P_\Omega = P_\Omega - \bar{P}_\Omega$. Second, they are strongly skewed toward the negative values, and third, they exhibit exponential tails. The upper inset in Fig. 1 presents the reduced average injected power versus Wi. The plot exhibits a powerlike dependence in the elastic turbulence regime according to the fit: $\bar{P}/\bar{P}_{\rm lam} \propto {\rm Wi}^{0.49\pm0.05}$, where $\bar{P}_{\rm lam}$ is the injected power before the transition. The lower inset in Fig. 1 shows the dependence of the reduced rms of the power fluctuations, $P^{\rm rms}/P^{\rm rms}_{\rm lam}$ on Wi, together with the fit $\propto {\rm Wi}^{3.2\pm0.3}$. In Fig. 2 we present PDFs of the normalized accelerations calculated from the temporal LDV measurements, $[Y(t) - Y_{\rm av}]/Y_{\rm rms}$, where $Y(t) \equiv \frac{dV(t)}{dt} V_{\rm av}^{-1}$. First, all data for several Wi values collapse on a single curve. Second, the PDFs show clear exponential tails. The left inset in Fig. 2 shows the Wi dependence of rms of the vorticity, $\omega_{\rm rms}$, scaled by $\lambda$, at several locations along the radius in the bulk of the flow. Since $\omega_{\rm rms} \sim \delta$, where $\delta$ is

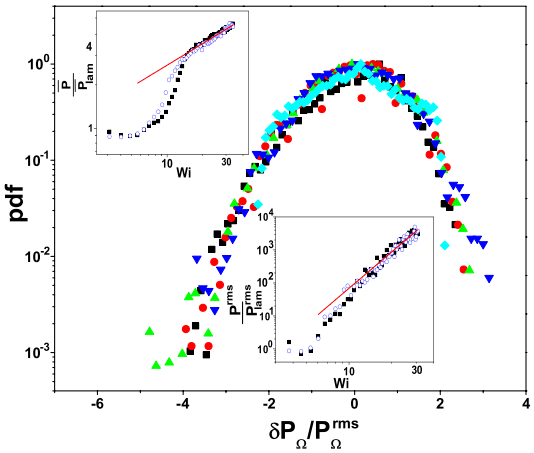


FIG. 1 (color online). PDFs of injected power fluctuations for various Wi: squares, 40; circles, 31.5; up triangles, 24; down triangles, 19; rhombs, 5. Upper inset: scaled average injected power vs Wi. Lower inset: scaled rms of injected power vs Wi. Squares present data taking in increasing Wi; open circles, in decreasing Wi.

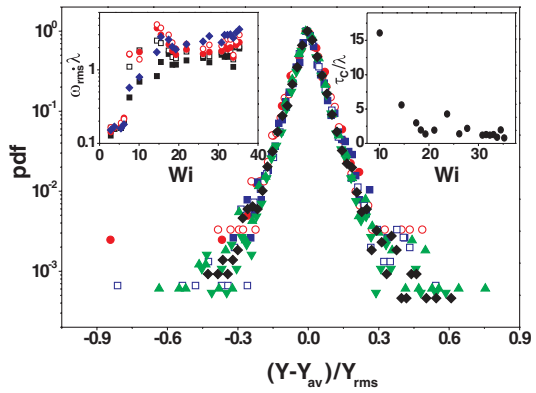


FIG. 2 (color online). PDFs of normalized accelerations for various Wi: full circles, 14; open circles, 16.2; full squares, 19.8; open squares, 22.3; up triangles, 26.3; down triangles, 30.7; rhombs, 38.9. Left inset: dependence of the scaled rms of vorticity, $\omega_{\rm rms}\lambda$, on Wi at several locations along radius $r/R_c$: full squares, 0.2; open squares, 0.33; full circles, 0.4; open circles, 0.5; rhombs, 0.66. Right inset: dependence of the scaled velocity correlation time, $\tau_c/\lambda$, on Wi.

the Lyapunov exponent of the Lagrangian trajectories, its saturation in the elastic turbulence regime at Wi between 15 and 35 is consistent with the recent theoretical prediction though here $\omega_{\rm rms}\lambda > 1$ [6,7]. The latter means that, probably, the nonlinearity of polymer elasticity also contributes to the saturation of the elastic stress [15,16]. The saturation of both $\delta$, already reported [17], and the reduced velocity correlation time, $\tau_c/\lambda$, shown in the right inset in Fig. 2 in the same range of Wi, just reinforces the observation. We investigated in detail the structure of horizontal (near the top and bottom plates) and vertical (near the walls) velocity boundary layers at different values of Wi and fluid viscosity. In Fig. 3 we present the average azimuthal velocity profiles in a vertical plane at $r = 3R_c/4$ normalized by its value at the disk, $\tilde{V}_\theta(z/d) = V_\theta(z/d)/V_\theta^{\rm up}$, obtained by the LDV measurements in 65% saccharose solution at various $\Omega$. The data for different $\Omega$ collapse on a single curve after subtracting for each curve the $z$ dependence of the average velocity in the bulk. Similar velocity profiles were also obtained for 60% and 50% saccharose solutions. It is clear from the data that the boundary layer width, $w$, is independent of $\Omega$ for each solution, and varies as a function of the solution viscosity as $w \propto \eta^{0.26\pm0.05}$ (upper inset in Fig. 3). In the lower inset in Fig. 3 we show the rms of the azimuthal velocity gradients, $(\frac{\partial V_\theta}{\partial r})_{\rm bl}^{\rm rms}$, scaled by $\lambda$ and measured by PIV at $z = d/2$ in the vertical boundary layer of $d = 1$ cm cell height versus Wi. This was obtained from widths of distributions of azimuthal velocity slopes in the boundary layer. We find a clear increase of $(\frac{\partial V_\theta}{\partial r})_{\rm bl}^{\rm rms}\lambda \gg 1$ with Wi in the boundary layer in contrast to its saturation in the bulk (see Fig. 2) in the same range of Wi. Moreover, a well-pronounced peak in the radial dependence of $(\frac{\partial V_\theta}{\partial r})^{\rm rms}$ inside the boundary layer width was also observed. Its position does not depend on Wi, while its normalized values at the peak, $(\frac{\partial V_\theta}{\partial r})_{\rm max}^{\rm rms}\lambda$, are up to 2 orders of magnitude larger than the bulk value, (the data are not shown, see Ref. [18]). Using PIV data one can also calculate the structure functions of the velocity gradients as $S_p(r) = \langle|\frac{\partial V_\theta(r_0+r)}{\partial r} - \frac{\partial V_\theta(r_0)}{\partial r}|^p\rangle_{r_0}$ shown in Fig. 4. The structure functions of $\omega$, $P_\Omega$, and $P_T$, were also calculated. In analogy with inertial turbulence, we looked for a scaling of $S_p(r)$ in the range of scales corresponding to the algebraic decay of the velocity spectra [1,2,14,19] in the form: $S_p(r) = r^{\zeta_p}$. The dependence of the normalized scaling exponent, $\zeta_p/\zeta_4$, on the order of the

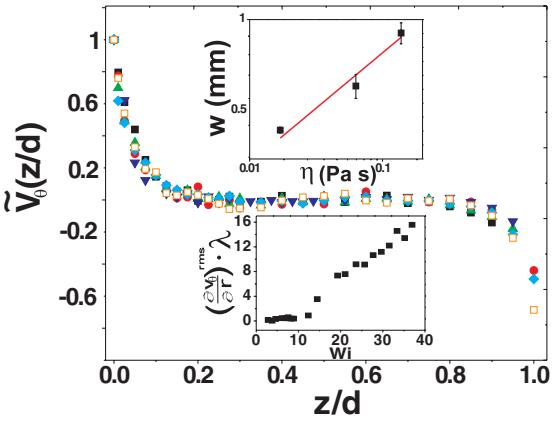


FIG. 3 (color online). Normalized vertical profile of average azimuthal velocity for several values of $\Omega$ s$^{-1}$: full squares, 5; circles, 4; up triangles, 3; down triangles, 2.5; rhombs, 2; open squares, 1.5. Upper inset: $w$ vs solution viscosity; solid line is the fit $w \propto \eta^{0.26\pm0.05}$. $w$ is defined from intersection of linear fits for bulk and near-the-wall parts of velocity profiles. Lower inset: scaled rms of velocity gradient in the boundary layer vs Wi.

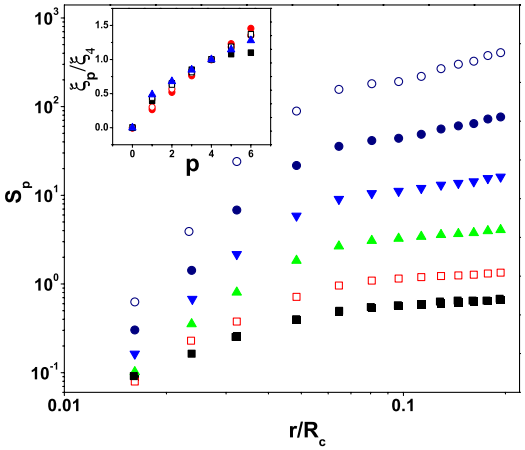


FIG. 4 (color online). Structure functions of velocity gradient of $p$ order up to $p = 6$ as a function of the scaled radius. Inset: normalized scaling exponent vs $p$ for: injected power $P_\Omega$, full circles; injected power $P_T$, open circles; passive scalar, full squares; vorticity, open squares; velocity gradient, up triangles.

structure functions, $p$, is presented in the inset in Fig. 4 for all flow parameters mentioned above. The dependencies are rather close to that obtained for a passive scalar in elastic turbulence, based on our published data [14,20]. So, all dependencies of $\zeta_p/\zeta_4$ on $p$ are nonlinear which implies anomalous scaling and strong deviation from the Gaussian distribution.

How can we put together all these pieces of information? We postulate that the elastic stress is accumulated near the wall due to a constant flux of momentum from the upper boundary. Its excess is intermittently injected into the bulk. Every time elastic stress is injected from the boundary layer into the bulk, the power on the disc reduces. This is a possible origin of the observed exponential tails and of the skewness toward small values of PDFs of the injected power $\delta P_\Omega/P_\Omega^{\mathrm{rms}}$. The exponential tails in the PDF of the velocity gradients can be also explained in the same way. Symmetry of the PDF is preserved due to injections from both the upper and lower boundary layers. However, the most surprising and striking feature of elastic turbulence observed is the presence of the velocity boundary layer and the emergence of a new length scale.

The picture presented is in close analogy with the turbulent advection of a passive scalar in the Batchelor regime in a finite channel flow, where the excess of tracer from the boundary layer is intermittently injected into the bulk [20,21]. In this case, the mixing boundary layer and the new length scale appear due to the existence of a small parameter, the inverse Peclet number, $\mathrm{Pe}^{-1} = (D/V^{\mathrm{rms}}L) \ll 1$, where $D$ is the diffusion constant and $L$ is the channel width. Then, as predicted theoretically [21] and confirmed experimentally [20], the mixing boundary layer is found to be $l_{\mathrm{mix}} \propto \mathrm{Pe}^{-1/4}$.

Exploring further the analogy with the passive scalar problem, one can suggest that here also a small parameter in the problem defines a new length scale. Since the diffusion does not play any significant role in elastic turbulence, $K \equiv (\frac{\partial V_\theta}{\partial r})^{\mathrm{rms}}_{\mathrm{bulk}}/(\frac{\partial V_\theta}{\partial r})^{\mathrm{rms}}_{\mathrm{bl}} \ll 1$ can be considered as a small parameter. This small parameter also defines the ratio of polymer stretching in the bulk and in the boundary layer. Thus, the width of the boundary layer for the elastic stress, based on these considerations and on the experimental observation, scales like $w \propto K^\alpha \eta^{1/4}$. The analogy in the statistics and scaling of the passive scalar and of the elastic stress due to advection by a smooth random flow is reinforced by the similarity in the statistical behavior presented in Fig. 4.

The saturation of the elastic stress in the bulk naturally explains the scaling $\frac{\bar{P}}{\bar{P}_{\mathrm{lam}}} \sim \mathrm{Wi}^{0.49}$, presented in Fig. 1. Indeed, the injected power is proportional to the torque. The latter is just the shear stress averaged over the upper plate, and in the elastic turbulence regime it is solely defined by the elastic stress in the bulk [5]. As we discussed, in elastic turbulence the latter saturates [see Eq. (3)]. On the other hand, it was found that due to shear thinning of the polymer solution used, one gets $\lambda \sim \Omega^{-0.3}$ [11,14]. Thus, the theoretically expected growth of the mean injected power with respect to its laminar value, $\bar{P}_{\mathrm{lam}}$, should be solely due to the bulk elastic stress and have the following power-law scaling: $\frac{\bar{P}}{\bar{P}_{\mathrm{lam}}} \sim \tau_p \sim \frac{\eta}{\lambda} \sim \Omega^{0.3} \sim \mathrm{Wi}^{0.43}$. This is rather close to the experimentally observed scaling.

We thank M. Chertkov and V. Lebedev, for numerous discussions. This work was supported by grants of the Israel Science Foundation, the Binational US-Israel Foundation, and the Minerva Center for Nonlinear Physics of Complex Systems.

[1] A. Groisman and V. Steinberg, Nature (London) **405**, 53 (2000).
[2] A. Groisman and V. Steinberg, New J. Phys. **6**, 29 (2004).
[3] A. Groisman and V. Steinberg, Nature (London) **410**, 905 (2001).
[4] L. D. Landau and E. M. Lifschitz, *Fluid Mechanics* (Pergamon Press, Oxford, 1987).
[5] A. Groisman and V. Steinberg, Phys. Rev. Lett. **86**, 934 (2001).
[6] E. Balkovsky, A. Fouxon, and V. Lebedev, Phys. Rev. E **64**, 056301 (2001).
[7] A. Fouxon and V. Lebedev, Phys. Fluids **15**, 2060 (2003).
[8] M. Chertkov, Phys. Fluids **10**, 3017 (1998).
[9] A. Schekochihin *et al.*, Astrophys. J. **612**, 276 (2004).
[10] R. G. Larson, E. S. G. Shaqfeh, and S. J. Muller, J. Fluid Mech. **218**, 573 (1990).
[11] A. Groisman and V. Steinberg, Phys. Fluids **10**, 2451 (1998).
[12] G. K. Batchelor, J. Fluid Mech. **5**, 113 (1959).
[13] T. Burghelea, E. Segre, and V. Steinberg, Phys. Fluids **17**, 103101 (2005).
[14] T. Burghelea, Ph.D. thesis, Weizmann Institute of Science, 2005 (unpublished).
[15] E. Balkovsky, A. Fouxon, and V. Lebedev, Phys. Rev. Lett. **84**, 4765 (2000).
[16] M. Chertkov, Phys. Rev. Lett. **84**, 4761 (2000).
[17] T. Burghelea, E. Segre, and V. Steinberg, Europhys. Lett. **68**, 529 (2004).
[18] T. Burghelea, E. Segre, and V. Steinberg (unpublished).
[19] V. Steinberg, in *Handbook of Experimental Fluid Dynamics* (Springer Verlag, Berlin, 2005), Chap. C2.3.
[20] T. Burghelea, E. Segre, and V. Steinberg, Phys. Rev. Lett. **92**, 164501 (2004); T. Burghelea, E. Segre, I. Bar-Joseph, A. Groisman, and V. Steinberg, Phys. Rev. E **69**, 066305 (2004).
[21] M. Chertkov and V. Lebedev, Phys. Rev. Lett. **90**, 034501 (2003); V. Lebedev and K. Turitsyn, Phys. Rev. E **69**, 036301 (2004).